Coexistence of metallic and insulating channels in compressed YbB_{6}

Jianjun Ying, Lingyun Tang, Fei Chen, Xianhui Chen, and Viktor V. Struzhkin

Phys. Rev. B **97**, 121101 — Published 2 March 2018

DOI: 10.1103/PhysRevB.97.121101

Coexistence of metallic and insulating channels in compressed YbB_6

Jianjun Ying,[1,2] Lingyun Tang,[3] Fei Chen,[4] Xianhui Chen,[4,5] and Viktor V. Struzhkin[1]

[1]*Geophysical Laboratory, Carnegie Institution of Washington, Washington, DC 20015, USA.*
[2]*HPCAT, Geophysical Laboratory, Carnegie Institution of Washington, Argonne, Illinois 60439, USA*
[3]*High Pressure Synergetic Consortium (HPSynC), Geophysical Laboratory, Carnegie Institution of Washington, Argonne, USA*
[4]*Hefei National Laboratory for Physical Sciences at Microscale and Key Laboratory of Strongly-Coupled Quantum Matter Physics, Chinese Academy of Sciences, School of Physical Sciences, University of Science and Technology of China, Hefei 230026, China*
[5]*Collaborative Innovation Center of Advanced Microstructures, Nanjing 210093, China*

(Dated: February 20, 2018)

It remains controversial whether compressed YbB_6 material is a topological insulator or a Kondo topological insulator. We performed high pressure transport, X-ray diffraction, X-ray absorption spectroscopy and Raman scattering measurements on YbB_6 samples in search for its topological Kondo phase. Both high pressure powder XRD and Raman measurements show no trace of structural phase transitions in YbB_6 up to 50 GPa. The nonmagnetic Yb^{2+} gradually change to magnetic Yb^{3+} above 18 GPa concomitantly with the increase of resistivity. However, the transition to the insulating state occurs only around 30 GPa, accompanied by the increase in the shear stress, and anomalies in the pressure dependence of the Raman T_{2g} mode and in B atomic position. The resistivity at high pressures can be described by a model taking into account coexisting insulating and metallic channels, with the activation energy for the insulating channel about 30 meV. We argue that YbB_6 may become a topological Kondo insulator at high pressures above 35 GPa.

PACS numbers: 74.62.Fj, 74.25.F-, 71.27.+a

Topological insulators(TIs) represent the newly discovered phase of matter with insulating bulk state having topologically protected metallic surface state due to the time-reversal symmetry and strong spin-orbital interaction[1–10]. Recently, one of the new TIs, named Topological Kondo insulator(TKI) was proposed by combining the strong electron correlations with the topological characteristics. Theoretical calculations predicted mixed valence material SmB_6 as the first example of TKI[11], produced by hybridization of the 5d conduction electrons with the local 4f electrons at low temperatures. Indeed, topological surface state has been confirmed in this material by many experiments such as transport[12–14], angle resolved photoemission(ARPES)[15–17], quantum oscillations[18], and point-contact spectroscopy measurements[19].

After successful theoretical prediction of TKI for SmB_6, a mixed valence YbB_6 (being a structural analog of SmB_6), was also predicted to be a TKI, but with a three times larger band gap[20]. However, unlike SmB_6, the Yb ion in YbB_6 is nearly divalent, and very small portion of Yb^{3+} was detected in the sample[21,22]. These experimental findings are in strong disagreement with the mixed valence state predicted by the theoretical work[20]. The insignificant portion of the higher valence state in YbB_6 may explain controversies in the angle-resolved photoelectron spectroscopy(ARPES) measurements which did not reach consensus yet on the topological insulator properties in this material[23–26]. Experimentally, no surface conduction channel has been observed in this material[12]. YbB_6 was suggested to have only a topologically trivial *p-d* semiconducting band gap, and hence it is a conventional insulator under ambient pressure conditions[27]. Thus, in order to realize the Kondo insulating state with the topological insulator properties in this material, we need to change the valence of Yb ions. High pressure is a clean method to change the electronic properties and also an effective way to tune the valence without introducing any impurities. Since the ionic radius of Yb^{3+} is smaller than Yb^{2+}, the application of high pressure will usually tune the nomagnetic Yb^{2+} to magnetic Yb^{3+}. Thus, by applying external pressure, we can tune the nearly divalent YbB_6 system to a mixed valence state, and we may anticipate to observe the Kondo insulating state or topological Kondo insulating state in YbB_6 under pressure. Previously, the high pressure work on YbB_6 below 30 GPa indeed found the portion of Yb^{3+} starting to increase at high pressure and the insulating state was found to emerge above 15 GPa[28]. However, the topological property of the insulating phase along with the valence of Yb are still uncertain, especially at higher pressures.

Here, we performed high pressure transport, X-ray diffraction(XRD), X-ray absorption spectroscopy (XAS) and Raman scattering measurements on YbB_6. The detailed description of experimental methods is provided in Supplementary Materials. Contrary to previous studies, we do not find evidence for two quantum transitions around 10 GPa and 15 GPa, reported in[28] from transport measurements in non-hydrostatic conditions. Moreover, we observe a pressure-induced transition to the insulating state only around 30 GPa at room temperature (around 27 GPa at low temperature). At room temperature, this transition is accompanied by the increase in the shear

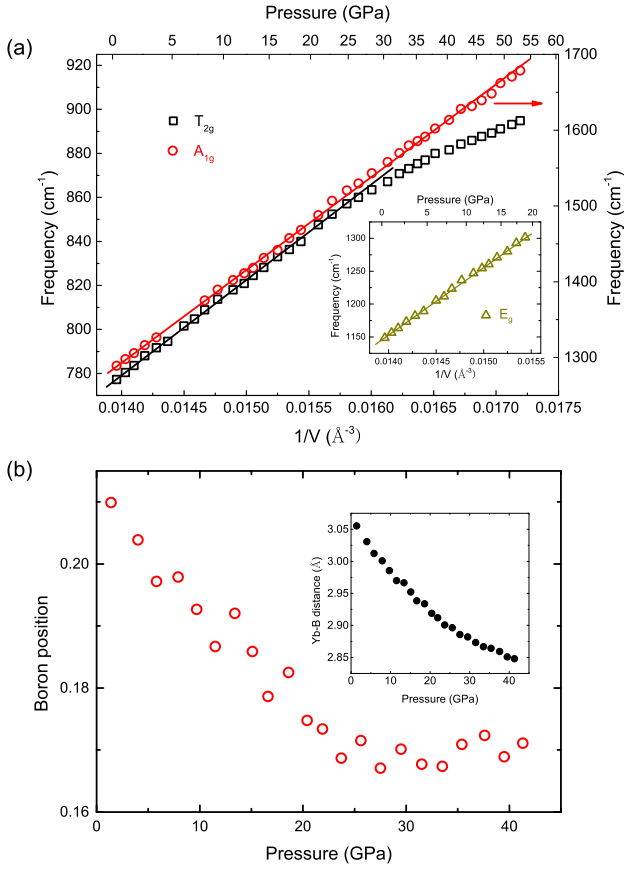

FIG. 1: (color online). (a) Raman-active phonon modes vs. 1/V in YbB_6. The slope of the A_{1g} mode does not show any anomalies up to 50 Gpa. However, the T_{1g} mode deviates from the linear behavior above 25 GPa. The E_g mode shows linear behavior below 20 GPa. (b) The pressure dependence of B atomic position which was calculated from the lattice parameter and Yb-B distance deduced from XANES measurements. The B atomic position decreases when pressure is increased to 25 GPa, and stays nearly constant above 25 GPa.

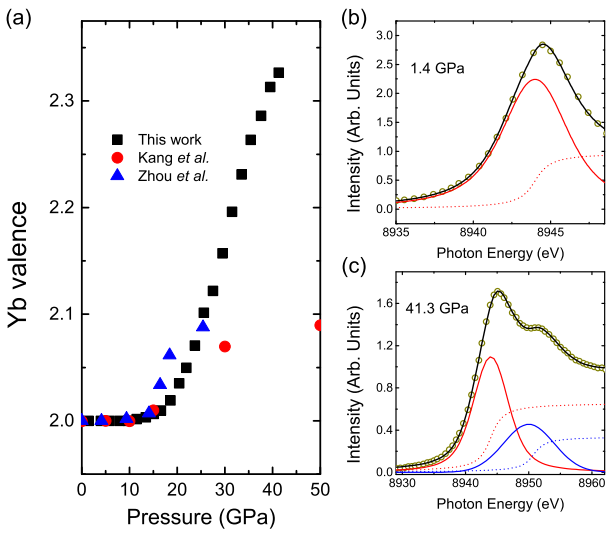

FIG. 2: (color online). (a) The pressure dependence of the valence of Yb as deduced from the XANES measurements. The valence of Yb is nearly 2+ at low pressure. It starts increasing above 18 GPa. The red circles and blue triangles represents the values taken from the previous theoretical calculation and experimental work, respectively.[27,28] (b) The results of XANES fits under the pressure of 1.4 GPa. Only Yb^{2+} component is used to fit the data. (c) A typical fitting result in the mixed-valence state. Both Yb^{2+} and Yb^{3+} are included to fit the data.

stress, and by anomalies in the pressure dependence of the Raman T_{2g} mode and in B atomic position, which follow from the changes in the electronic structure. We find a region with metallic conductivity at low temperatures only above 35 GPa, which was not found in previous work performed in a limited pressure range ($\sim$ 26 GPa)[28]. We argue that such novel insulating behavior is related to the topological Kondo insulating state, due to the valence crossover of Yb ions. This finding warrants further investigations to confirm the TKI phase at high pressures.

The divalent and trivalent metal hexaborides (MB_6) crystallize in the cubic CsCl structure (space group Pm3m) with one molecule per unit cell[30]. Ionic displacements of three Raman-active phonon modes (T_{2g}, E_g and A_{1g}) in the cubic symmetry[31]. Both the high pressure polycrystalline XRD and Raman spectroscopy measurements confirm the absence of structural transitions below 50 GPa. However, we do observe anomalies in the linewidths of the x-ray diffraction lines (101) and (111) around 30 GPa, while no anomalies are found in the linewidth of (100) reflection[31]. This points to a possible shear stress increase around that pressure, due to the softening of the shear modes. Such softening would affect mostly the distances between (101) or (111) lattice planes (corresponding to the deformations along the face or the body diagonal, respectively). Another possibility is lowering of the symmetry due to a shear distortion, which may be too small to be resolved in our x-ray measurements. However, such scenario is not supported by our Raman data. We can plot the Raman shift of A_{1g}, E_g and T_{2g} modes as a function of the reciprocal volume of the unit cell as shown in Fig. 1(a). No anomaly was observed in the A_{1g} mode, however, the T_{2g} mode (which has vibration eigenvectors typical for a shear mode) starts to deviate from the linear behavior above 25 GPa, and broadens around 30 GPa. This behavior is suggestive of a stress-induced broadening, rather than of a mode splitting, which would be observed in a case of a structural distortion. The E_g mode does not show any anomalies below 20 GPa as shown in the inset of Fig. 1(a), and we can not obtain reliable mode frequencies above 20 GPa due to the overlap of this mode with the Raman response of the diamond anvil.

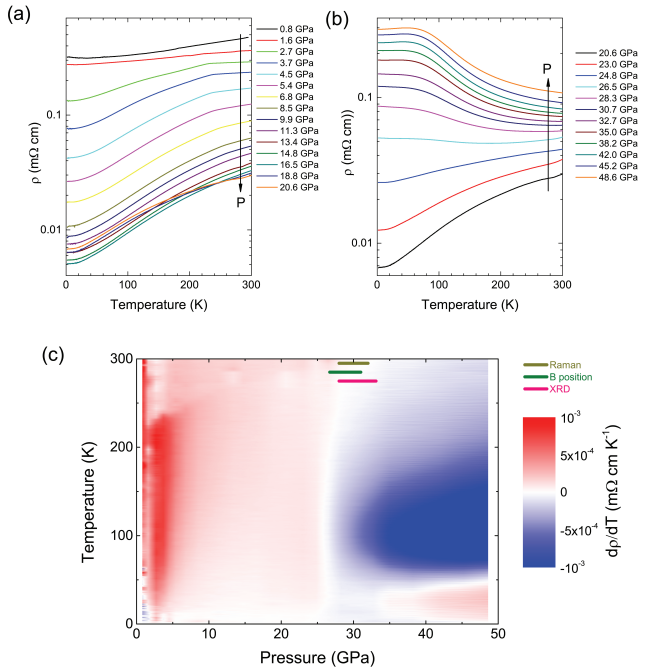

FIG. 3: (color online). The temperature dependence of the resistivity under various pressures. (a)The resistivity is gradually suppressed below 18 GPa and starts to increase above 18 GPa due to the contribution of magnetic scattering. (b) The resistivity continuously increases with increasing pressure and starts to exhibit insulating behavior above 27 to 30 GPa from low to room temperature. However, the resistivity at low temperature shows metallic behavior above 35 GPa, which is completely different when compared to the other trivial insulators. (c) Phase diagram of the YbB_6 under pressure. The red and blue area represent the metallic and insulating behavior, respectively. The colored bars represent anomalies in Raman T_2g mode (beige), B atomic position (green) and in x-ray diffraction linewidth (red) at room temperature (the bars are are shifted vertically for better visibility).

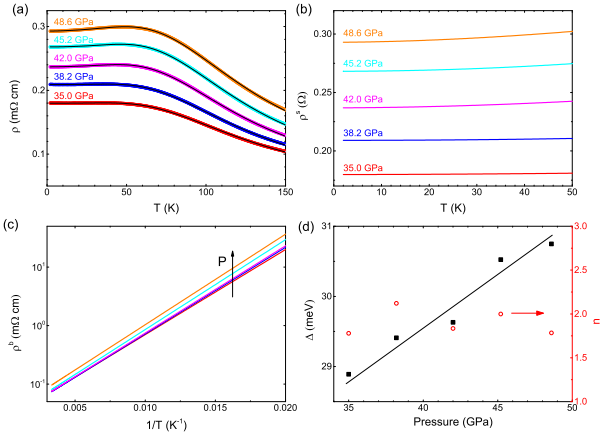

FIG. 4: (color online).(a) The fitting results for the resistivity above 35 GPa, the two channel model is used in the fits. The black lines are the fitting curves. The metallic surface channel ρ^s (b) and insulating bulk channel ρ^b (c) as deduced from the fitting results at various pressures. (d) The pressure dependence of the parameters Δ and n determined from the fits.

In order to clarify the valence of Yb ions and their effect on the T_{2g} mode anomaly under pressure, we performed XAS measurements on YbB_6 under pressure. The XAS can be divided into two regions: x-ray absorption near-edge spectroscopy (XANES) and extended x-ray absorption fine-structure spectroscopy (EXAFS). XANES is strongly sensitive to formal oxidation state and coordination chemistry of the absorbing atom, while the EXAFS is used to determine the distances, coordination number, and species of the neighbors of the absorbing atom. Clear oscillations were detected in the region of EXAFS part[31]. Thus, we can deduce the distance between the neighbors and the absorbing atom. Through analysis of the EXAFS by using the Demeter software[32] we obtained the pressure dependence of Yb-B distances as shown in the inset of Fig. 1(b). Thus, the B position can be calculated from the lattice parameter and Yb-B distance. The B position first decreases with increasing pressure, and then stays nearly constant above 26 GPa as shown in Fig. 1(b). This pressure is consistent with the pressure where T_{2g} mode has an anomaly - Fig. 1. These results indicate that the Yb-B bond is more compressible than the B-B bond below 26 GPa, and at higher pressures B-B and Yb-B bonds have comparable compressibility.

The sharp peak around 8944 eV and the anomaly around 8950 eV of the XANES part represent the Yb^{2+} component and Yb^{3+} component[31], respectively. Our data clearly shows that the Yb^{3+} component gradually increases and Yb^{2+} component decreases with pressure increase. We assumed the Voigt functions for fitting both the Yb^{2+} and Yb^{3+} components. The arctangent backgrounds were used for the fitting. The typical fitting results are shown in Fig. 2(b) and (c). The Yb valence can be calculated by $2 + I_{3+}/(I_{2+} + I_{3+})$, where I_{2+} and I_{3+} are intensities of the Yb^{2+} and Yb^{3+} components, respectively. The pressure dependence of Yb valence is shown in Fig. 2(a). The Yb valence is nearly 2+ at low pressure, but it starts to increases above 18 GPa. The value of the estimated Yb valence is comparable to the previous experimental result[28], however, it is much higher than the value predicted by the theoretical calculations[?] . The average valence at 30 GPa is 2.17, suggesting that the insulalting state does form only when approximately 17% of the Yb ions switched their valence to +3.

The high pressure resistivity of YbB_6 shows metallic behavior at low pressure as shown in Fig.3 (a). The resistivity was continuously suppressed in the pressure range below 18 GPa. It is known that YbB_6 is a doped semiconductor[22] at ambient pressure conditions. Application of pressure would usually decrease the band gap,

thus the resistivity would be continuously decreasing and the system would become a metal. Indeed, this behavior is observed below 18 GPa in YbB_6. However, during further increase of pressure above 18 GPa the resistivity starts to increase. Such behavior correlates with the increase of the Yb valence above 18 GPa, since the magnetic scattering on Yb^{3+} ions would enhance the resistivity. However, the resistivity start to exhibit insulating behavior only above ∼27 GPa. Unlike the ordinary insulators, the resistivity stops increasing when the temperature drops below ∼50 K. We can map out the phase diagram as a function of $d\rho/dT$ as shown in Fig. 3(c). The red and blue areas represent the metallic and insulating behavior, respectively. Above 35 GPa, the resistivity shows insulating behavior, however, metallic behavior reemerges at low temperature under high pressure. As we know, for an ideal topological insulator, resistivity behavior at high temperature is dominated by the insulating gap of the bulk material, while its metallic surface will provide significant contribution to the conductivity only at low temperatures. We expect that the valence change of the Yb ions would tune this non-magnetic system to a Kondo lattice system at high pressure, thus a Kondo insulting state would possibly emerge. Such behavior in YbB_6 is quite similar to its samarium analog material SmB_6, which is suggested to be a topological Kondo insulator. These results indicate that the system evolves from a metallic state to an non-trivial insulating state above 27 GPa. This critical pressure is consistent with the pressure where both the T_{2g} Raman mode and B atomic position show anomalous behavior, which may be triggered by the reconstruction of the electronic states in the material. The correlation between the structural parameters and transport properties needs further theoretical investigations.

For a topological insulator, the measured resistivity can be described by a two channel model: $1/\rho=1/\rho^s d+1/\rho^b$, d is the thickness of the sample, the surface resistivity ρ^s can be treated as $\rho^s=\rho_0^s+AT^n$, the insulating state resistivity is $\rho^b=B\exp(\Delta/T)$. Actually, we can fit the resistivity above 35 GPa by using this two channel model quite well as shown in Figure 4(a). Fig. 4 (b) and (c) show the pressure dependence of ρ^s and ρ^b, respectively. The value of the parameter n is close to 2 as shown in Fig. 4(d), which implies that the metallic state can be described by the Fermi liquid theory. The fitting parameter Δ is about 30 meV, which is close to the theoretically calculated value of the band gap for the mixed valence YbB_6[20] at ambient pressure. The parameter Δ slightly increases with increasing pressure. Our resistivity results are suggestive of the scenario when a trivial insulator converts to a non-trivial topological insulator by continuously adjusting a control parameter (pressure). The coexistence of the metallic and insulating channels indicates that the high pressure insulating state is possibly a topological insulator.

Our resistivity results clearly support the topological phase transition in YbB_6 under pressure. Due to the increasing valence of the Yb ions at high pressure, the YbB_6 will meet the criterion of mixed valence compound. Thus, the conduction electrons (5d-electrons) would hybridize with localized electrons (4f-electrons) and open up a narrow band gap as the theoretical calculation predicts[20]. This might be the reason for resistivity to exhibit insulating behavior above 27 GPa. At high pressures, the resistivity below 150 K can be fitted using the two channel model. The coexistence of the metallic and the insulating resistivity channels in the samples indicates that the system may have been turned into a TKI state. However, we are still in need of direct experimental methods to identify whether such metallic channels belong to the surface or to the bulk of the material under high pressure conditions. Another possibility of the coexistence of the metallic and insulating channels may due to phase separation due to the inhomogeneity under pressure. However, the resistivity around 28.3 GPa already shows insulating behavior at low temperature. We would expect that such insulating behavior should be more significant at higher pressures since the portion of the insulating phase should increase. However, the low temperature behavior becomes metallic at low temperature above 35 GPa. These observations exclude the phase separation assumption. Based on arguments provided above, we argue that the origin of such non-trivial insulating state may be indeed due to the evolution of the system towards a TKI state. The compression should increase the magnetism of Yb ions, thus the band gap of the Kondo insulating state would increase under pressure. Further experimental and theoretical work is needed to prove the existence of the TKI state in YbB_6 at high pressures. We notice that our resistivity behavior is quite different from the previous results[28], and extends to higher pressure range (above >25 GPa pressure limit in[28]), which provided us the opportunity to observe TKI-type conductivity above 30 GPa. The difference in resistivity measurements is mostly due to the fact that we used a liquid pressure medium which provides better hydrostatic pressure environment compared to the solid pressure medium which was used in the previous work[28]. For example, recent experiments confirm high sensitivity of the resistivity in SmB_6 to uniaxial stress[29]. Our XAS data and resistivity data were obtained using the same liquid pressure medium, which helps us to better compare the data resulting from different methods (Our XAS results are similar to the previous study since both studies used the liquid pressure medium for the XAS measurements[28]).

Previous calculations suggested that YbB_6 is a p-d overlap semimetal at high pressures[27]. However, the calculated valence of Yb in that work was much smaller than the experimental values at high pressures. Our results provide more accurate phase diagram, which will serve as a better guide for further theoretical calculations needed to check the topological properties of YbB_6 at high pressure. Hopefully, the theory will also help to explain the anomalies in the T_{2g} mode behavior and in B atomic position, and sensitivity to the shear stress,

which emerge concomitantly with the insulating state in the material.

In conclusion, we performed high pressure Raman scattering, XRD, XAS and transport measurements on YbB_6 samples. With increasing amount of the Yb^{3+} ions, the system gradually develops insulating behavior above 27∼30 GPa (at about 17% abundance of the Yb^{3+} ions according to our XAS data), when the anomalies are observed in the pressure dependence of the T_{2g} Raman mode, B atomic position, and linewidths of x-ray (101) and (111) reflections, suggestive of shear stress-induced broadening. The resistivity at high pressures above 35 GPa can be described by a model taking into account coexisting insulating and metallic channels, with the activation energy for the insulating channel about 30 meV, consistent with the theoretical calculation which assume it is mixed valence at ambient pressure. Our results suggest that the compressed YbB_6 may become topological Kondo insulator above 35 GPa. It remains to be seen if the chemical pressure, uniaxial strain or their combination could stabilize the topological Kondo insulator state in this family of materials closer to the ambient pressure and temperature conditions as was observed in previous work on SmB_6[29]. For future research it is also important that applied stress may have substantial influence on the TKI state in YbB_6, which may allow stabilize it in a strained multilayer material engineered for more practical applications at ambient pressure.

Acknowledgments

We thank Changyong Park for the help on the XAS experiment. High pressure experiments at HPCAT and at the Geophysical Laboratory were supported by DOE/BES under contract No. DE-FG02-99ER45775. Portions of this work were performed at HPCAT (Sector 16), Advanced Photon Source (APS), Argonne National Laboratory. HPCAT operation is supported by DOE-NNSA under Award No. DE-NA0001974, with partial instrumentation funding by NSF. The Advanced Photon Source is a U.S. Department of Energy (DOE) Office of Science User Facility operated for the DOE Office of Science by Argonne National Laboratory under Contract No. DE-AC02-06CH11357. Portions of this work were performed at GeoSoilEnviroCARS (The University of Chicago, Sector 13), Advanced Photon Source (APS), Argonne National Laboratory. GeoSoilEnviroCARS is supported by the National Science Foundation - Earth Sciences (EAR-1128799) and Department of Energy- GeoSciences (DE-FG02-94ER14466). This research used resources of the Advanced Photon Source, a U.S. Department of Energy (DOE) Office of Science User Facility operated for the DOE Office of Science by Argonne National Laboratory under Contract No. DE-AC02-06CH11357.

[1] M. Z. Hasan and C. L. Kane, Rev. Mod. Phys. **82**, 3045 (2010).
[2] X. L. Qi and S. C. Zhang, Rev. Mod. Phys. **83**, 1057 (2011).
[3] X. L. Qi and S. C. Zhang, Phys. Today **63**, 33 (2010).
[4] C. L. Kane and E. J. Mele, Phys. Rev. Lett. **95**, 146802 (2005).
[5] B. A. Bernig, T. L. Hughes, and S. C. Zhang, Science **314**, 1757 (2006).
[6] M. Konigm, S. Wiedmann, C. Brune, A. Roth, H. Buhmann, L. W. Molenkamp, X. L. Qi, and S. C. Zhang, Science **318**, 766 (2007).
[7] L. Fu and C. L. Kane, Phys. Rev. B **76**, 045302 (2007).
[8] D. Hsieh, D. Qian, L. Wray, Y. Xia, Y. S. Hor, R. J. Cava, and M. Z. Hasan, Nature (London) **452**, 970 (2008).
[9] Y. Xia, D. Qian, D. Hsieh, L. Wray, A. Pal, H. Lin, A. Bansil, D. Grauer, Y. S. Hor, R. J. Cava, and M. Z. Hasan, Nat. Phys. **5**, 398 (2009).
[10] H. Zhang, C. X. Liu, X. L. Qi, X. Dai, Z. Fang, and S. C. Zhang,, Nat. Phys. **5**, 438 (2009).
[11] F. Lu, J. Zhao, H. Weng, Z. Fang, and X. Dai, Phys. Rev. Lett. **110**, 096401 (2013).
[12] D. J. Kim, J. Xia, and Z. Fisk, Nat. Mater. **13**, 466 (2014).
[13] S. Wolgast, C. Kurdak, K. Sun, J. W. Allen, D. J. Kim, and Z. Fisk, Phys. Rev. B **88**, 180405 (2013).
[14] F. Chen, C. Shang, Z. Jin, D. Zhao, Y. P. Wu, Z. J. Xiang, Z. C. Xia, A. F. Wang, X. G. Luo, T. Wu, and X. H. Chen, Phys. Rev. B **91**, 205133 (2015).
[15] J. Jiang, S. Li, T. Zhang, Z. Sun, F. Chen, Z. R. Ye, M. Xu, Q. Q. Ge, S. Y. Tan, X. H. Niu, M. Xia, B. P. Xie, Y. F. Li, X. H. Chen, H. H. Wen, and D. L. Feng, Nature Comm. **4**, 3010 (2013).
[16] M. Neupane, N. Alidoust, S. Y. Xu, T. Kondo, Y. Ishida, D. J. Kim, Chang Liu, I. Belopolski, Y. J. Jo, T. R. Chang, H. T. Jeng, T. Durakiewicz, L. Balicas, H. Lin, A. Bansil, S. Shin, Z. Fisk, and M. Z. Hasan, Nat. Commun. **4**, 2991 (2013).
[17] N. Xu, X. Shi, P. K. Biswas, C. E. Matt, R. S. Dhaka, Y. Huang, N. C. Plumb, M. Radovi?, J. H. Dil, E. Pomjakushina, K. Conder, A. Amato, Z. Salman, D. McK Paul, J. Mesot, H. Ding, and M. Shi, Phys. Rev. B **88**, 121102(R) (2013).
[18] G. Li, Z. Xiang, F. Yu, T. Asaba, B. Lawson, P. Cai, C. Tinsman, A. Berkley, S. Wolgast, Y. S. Eo, Dae-Jeong Kim, C. Kurdak, J. W. Allen, K. Sun, X. H. Chen, Y. Y. Wang, Z. Fisk, and Lu Li, Science **346**, 1208-1212 (2014).
[19] X. Zhang, N. P. Butch, P. Syers, S. Ziemak, Richard L. Greene, and J. Paglione, Phys. Rev. X **3**, 011011 (2013).
[20] H. Weng, J. Zhao, Z. Wang, Z. Fang, and X. Dai, Phys. Rev. Lett. **112**, 016403 (2014).
[21] A. Aprea, A. Maspero, N. Masciocchi, A. Guagliardi, A. F. Albisetti, and G. Giunchi, Solid State Sci. **21**, 32 (2013).
[22] J. M. Tarascon, J. Etourneau, P. Dordor, P. Hagenmuller, M. Kasaya, and J. M. D. Coey, J. Appl. Phys. **51**, 574 (1980).
[23] M. Xia, J. Jiang, Z. R. Ye, Y. H. Wang, Y. Zhang, S. D. Chen, X. H. Niu, D. F. Xu, F. Chen, X. H. Chen, B. P. Xie, T. Zhang, and D. L. Feng, Sci. Rep. **4**, 5999 (2014).
[24] M. Neupan, S. Y. Xu, N. Alidoust, G. Bian, D. J. Kim,

C. Liu, I. Belopolski, T. R. Chang, H. T. Jeng, T. Durakiewicz, H. Lin, A. Bansil, Z. Fisk, and M. Z. Hasan, Phys. Rev. Lett. **114**, 016403 (2015).

[25] N. Xu, C. E. Matt, E. Pomjakushina, J. H. Dil, G. Landolt, J.-Z. Ma, X. Shi, R. S. Dhaka, N. C. Plumb, M. Radovic, V. N. Strocov, T. K. Kim, M. Hoesch, K. Conder, J. Mesot, H. Ding, and M. Shi, arXiv:1405.0165 (2014).

[26] E. Frantzeskakis, N. de Jong, J. X. Zhang, X. Zhang, Z. Li, C. L. Liang, Y. Wang, A. Varykhalov, Y. K. Huang, and M. S. Golden, Phys. Rev. B **90**, 235116 (2014).

[27] Chang-Jong Kang J. D. Denlinger, J. W. Allen, Chul-Hee Min, F. Reinert, B. Y. Kang, B. K. Cho, J.-S. Kang, J. H. Shim, and B. I. Min, Phys. Rev. Lett. **116**, 116401 (2016).

[28] Y. Zhou D. Kim, P. Rosa, Q. Wu, J. Guo, S. Zhang, Z. Wang, D. Kang, W. Yi, Y. Li, X. Li, J. Liu, P. Duan, M. Zi, X. Wei, Z. Jiang, Y. Huang, Y. Yang, Z. Fisk, L. Sun, and Z. Zhao, Phys. Rev. B **92**, 241118(R) (2015).

[29] A. Stern, M. Dzero, V.M. Galitski, Z. Fisk, J. Xia, Nature Materials **16**, 708 (2017).

[30] M. Ishii, M. Aono, S. Muranaka, S. Kawai, Solid State Commun. **20**, 437 (1976).

[31] See Supplemental Material at [url] for details of the experiments.

[32] B. Ravel and M. Newville, J. Synchrotron Rad. **12**, 537C541 (2005)